NUMERICAL SIMULATION OF THE GAS FLOW THROUGH THE RECTANGULAR CHANNEL WITH PERFORATED PLATE

by

Zoran J. MARKOVIĆ*[*]*, Milić D. ERIĆ, Rastko D. JOVANOVIĆ, and Ivan M. LAZOVIĆ

Vinca Institute of nuclear sciences, National Institute of the Republic of Serbia, University of Belgrade, Belgrade, Serbia

Original scientific paper
https://doi.org/10.2298/TSCI220426089M

The perforated plates are commonly used for gas flow control in the wide-angle diffusers of electrostatic precipitators of large power plants. Many studies dealt with the investigation of the effects of the perforated plate's geometry on flow parameters in the cases where incoming flow is perpendicular to the plate and the plate is covering the whole cross-section of the flowing channel. These results are partially applicable in cases where flow is inclined on the plate or when the plate is not occupying the whole cross-section of the channel. The subject of this work is a numerical investigation of flow through the rectangular channel with a perforated plate in various positions in the cross-section of the channel. The aim was to investigate the effect of the plate position on the flow. The perforated plates were modeled as thin porous media of finite thickness by using the directional loss model. Numerical experiments are carried out by using CFD software ANSYS CFX. Results of pressure drop and velocity distribution behind the plate are compared to the results of CFD simulation of the full 3-D plate model. In order to obtain a reasonable agreement both of the pressure drop and velocity distribution behind the plate when using a simplified thin porous plate model, the value of streamwise permeability of the plate had to be adjusted. The level of adjustments has determined iteratively and it depends on the plate position in the channel's cross-section.

Key words*: fluid-flow control, perforated plates, porous medium model, CFD*

Introduction

The new, restrictive best available technology requirements posed by EU Decision 2017/1442 [1] clearly define the need to take measures in order to improve the existing flue gas treatment installations. The electrostatic precipitator (ESP) is a device widely used for removing particles from hot flue gas generated in coal fired boilers. Electrostatic precipitation process is very effective in handling large volume of gases over a wide range of flue gas temperature, particle composition and inlet dust load, providing high total dust collection efficiency and low pressure drop through the ESP [2]. Due to flow vorticity in the interelectrode space and dust re-entrainment, establishing the flue gas flow uniformity through the dedusting

[*]Corresponding author, e-mail: zoda_mark@vin.bg.ac.rs

zone of the ESP chamber is a basic precondition for high dedusting efficiency of the ESP [3], espataially of particles smaller than 10 μm [4]. Flue gas enters the ESP chamber of complex inside geometry through the pyramidal wide-angle diffuser, which reduces gas velocities from between 16-24 m/s to a level of about 1.5 m/s (usual values for the ESP of Serbian 300 MW termal power plants). For reduction of the effects of flow separation, local jets, flow pulsation, or large-scale turbulence fluctuation upstream of the treatment zone of the ESP, it is common to install in the diffusor, perpendicularly to the main flow direction, screens in the form of perforated plates [5]. Maximum theoretical precipitator collection efficiency results from perfectly uniform gas velocity [6]. In order to obtain a uniform flow over the ESP inlet, determination of the adequate plate porosity (open area ratio) $f = A_O/A_P$ (A_O is area of the openings and A_P the area of the plate) and location of the perforated plates in the diffuser, are essential [7-9]. The dimensionless pressure loss coefficient, K, is the main characteristic of perforated plates [9-11] and relate to pressure drop Δp as $K = 2\Delta p/\rho U^2$ where U is the upstream velocity and ρ is the fluid density. The pressure loss coefficient, K, is associated with complex mixing processes which occur within the flow zone downstream the plate. Non-uniformity in the velocity and static pressure profiles increase as the porosity, f, decrease. Also, the amplitude of the velocity distribution non-uniformities is found to be greater for low porosity since the mixing process of the jets and surrounding fluid requires a greater axial distance to complete [11]. Results of experimental investigation [12] indicated that porosity, f, is the most influencing design parameter in terms of pressure drop, Δp, while the least effective are the Reynolds number and opening distribution pattern (pitch). The effect of porosity, f, thickness, t, and holes array, over a vide laminar and turbulent flow regimes, was numerically investigated for plate thickness, t, to hole diameter, D, ratios t/D of 0.5 and 1.0 [13]. Results showed that in the case of laminar flow the higher pressure drops was associated with thicker plate. In the case of turbulent flow, a thinner plate led to higher pressure drop while the distributor holes pattern is of little importance. Downstream length of the plate-induced flow disturbance, taken as the downstream distance from the plate at which the dimensionless pressure drop, Δp, has achieved 95% of its full value, was found to be in the order of one hole diameter in the case of laminar flow, and 5-6 diameters in the case of turbulent flow. A series of CFD-based numerical experiments was carried out at a microscopic, unit cell scale in order to investigate the effect of Reynolds number, plate porosity, f, thickness, t, surface roughness, and plate inclination angle on the flow pattern and pressure drop [14]. The design of experiments by using the Taguchi approach was implemented for perforated plates optimization over different parameters [15]. An analysis over the series of CFD simulation of the flow through the plate of different characteristics, for Reynolds number Re >4000, confirmed conclusions given in [12] that the most influencing parameter is porosity, f, and least effective is opening pitch.

Numerical modeling of the flow through the detailed structure of the perforated plate by using CFD [13-15] is computing resource and time processing demanding due to need to resolve each opening in a perforated plate with sufficient computational cells. This especially becomes important when doing optimization of geometrical parameters of the flow distributors forming a screen in the ESP diffusor in order to achieve as homogeny as possible flue gas flow in the ESP entrance, thus better dedusting characteristics of the ESP. Therefore, extensive researches of fluid-flow through the perforated plates have been carried out by using simplified thin porous media model [8, 16-19]. Model of the perforated plate is considered as homogenous porous material of finite thickness with additional source terms in the momentum equation. Additional terms are defined over directional permeability and internal resistance per unit thickness usually based on the results of experiments [8, 17-19] or by the

equation of fitting curve of numerically obtained results for the range of velocities [16]. With these parameters defined for the streamwise direction porous medium model is useful in the cases where incoming velocity is almost perpendicular to the perforated plate [16, 19]. A multi-scale method, based on the division of the large-scale ESP simulation into three steps (unit cell of internal components, a single ESP unit, and the entire ESP system) is applied for the modeling and optimization of a large ESP system in a coupled fashion [17]. By using CFD numerical simulation and empirical correlation for investigation of the effects of holes pitch of perforated plates of different porosities on flow uniformity, a small influence of the hole distribution and significant influence of the porosity f was found in the range of Re < 7000 [18]. In the frame of work [19] an indirect modeling approach based on the porous media model of the perforated plates of various porosities was applied, taking into account the structural elements between the plates. The influence of structural elements of the panel on the velocity distribution and pressure drop was numerically investigated and compared to the results obtained by the proposed porous panel model. Various relative errors of the numerical simulation by using a porous medium model compared to experimental results of the velocity distribution behind the perforated plate were reported.

The subject of this work was an investigation of the flow behind the perforated plate which does not cover the whole cross-section of the channel. This is a common situation in the diffusor of the ESP where perforated plates are placed in the screen's supporting frame that is not, for practical constructive reasons, extended up to the diffusor's walls. Therefore, there is always a passage between the screen's frame structure and the diffusor's wall that flue gas is *passing* through it due to lower resistivity to the flow. The aim was to achieve as much as possible coincident flow behind the plate modeled as porous medium regarding the pattern of the flow resolved by using detailed geometry of the perforated plate. The models with different values of the resistance coefficient were tested and the results were compared to the case of a detailed 3-D numerical model of the plate. The value of the resistance coefficient are defined by *trial and error*, starting from the value near theoretically defined one for the plate that is covering whole cross-section of the channel. The level of the flow similarity was estimated by comparing the pressure and velocity distributions along the selected horizontal and vertical lines and planes behind the plate. The values of the relative deviation of the pressure and velocity of the porous model regarding the corresponding values of the detailed model of the plate were not calculated in the scope of this work. The results of numerical calculaction showed that by adjusting resistance coefficient is possible to improve the matching of the flow patterns when applying the porous medium model and detailed plate model. The statistical processing of the results is inevitable for the future automation of the resistance coefficient value optimization process.

Numerical model

The seven different cases of rectangular channel geometry and the plate position inside of channel are considered, table presented on fig. 1 right. The length of the channel is 15 m along the *z*-axis with the main flow toward the positive orientation of the axis. The channel width/height is denoted as x_c and y_c, respectively. The plate is positioned 5 m from the inlet perpendicularly to the main flow. The origin of rectangular co-ordinate system is placed in the center of the plate vertical *x*-*y* cross-section. Symmetry conditions were employed (*z*-*x* and *z*-*y* symmetry) therefore only one-fourth of the whole domain was modelled, fig. 1 left. The perforated plate is of the thickness t = 5 mm, width x_p = 1000 mm (along axis *x*), and height y_p = 1500 mm (along axis *y*), with 20 × 18 rectangular 30 × 65 mm openings which form porosity

(open area ratio) of $f = 0.468$. The numerical model of the full-scale geometry of the perforated plate was designated as PP, while porous medium model of the perforated plate was designated as PO.

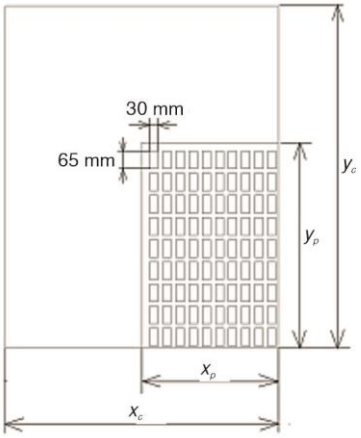

Case	$X_c = (x_c - x_p)/x_c$	$Y_c = (y_c - y_p)/y_c$
C1	0.0	0.0
C2	0.0	0.1
C3	0.5	0.4
C4	0.7	0.6
C5	0.8	0.6
C6	0.7	0.8
C7	0.8	0.8

Figure 1. The geometry of the channel cross-section and position of the perforated plate and geometrical characteristics of the numerical models

The relative position of the plate in the channel defined through the parameters X_c and Y_c were selected such to represent the case when plate is covering the cross-section of the channel (C1), as well as the case of the small (C2), medium (C3 and C4), and large (C5-C7) gaps relative to the plate dimension. In the present study, 3-D, steady-state turbulent flow was modeled using commercial CFD finite-volume-based software ANSYS CFX 2021R1. It was required to solve the RANS equation together with an eddy viscosity turbulence model. A shear stress transport *k-ω* turbulence model is chosen for its advantage in resolving flow separation and experimentally proved applicability validated in the frame of the work [13]. The governing equations for continuity, momentum and turbulent quantities, with associate model constants and parameters, are well documented elsewhere [20]. Dry air at 25 °C and 0.1 MPa with density $\rho = 1.185$ kg/m^3 and viscosity $\mu = 1.831 \times 10^{-5}$ Pa·s was assumed as incompressible and Newtonian. Inlet condition was set as velocity of value $V = 10$ m/s in direction normal to the inlet boundary [18, 20]. Turbulence intensity is derived from an empirical correlation for pipe flows as $I = 0.16 \cdot (\mathrm{Re_{Dh}})^{-1/8} = 4.5$ %. The conditions in the exit of the channel were set as pressure-outlet with $p_{st} = 0$ Pa average static pressure over the exit plane. The non-slip boundary condition was used on all the walls assumed to be with no roughness. When modeling perforated plate as porous media of finite thickness [16, 17], momentum equation was solved with an additional source term. One consider a streamwise-oriented co-ordinate system (x', y', z') such that z'-axis is aligned with the streamwise direction and the x', y' lie on the transverse plane. The streamwise directional momentum loses in z' direction is:

$$S_{M,z'} = -\frac{\mu}{K^S_{\mathrm{perm}}} U_{z'} - K^S_{\mathrm{loss}} \frac{\rho}{2} |U| U_{z'} \tag{1}$$

where K^S_{perm} [m^2] is the streamwise permeability, K^S_{loss} [m^{-1}] – the streamwise resistance loss coefficients, and $|U|$ – the gas velocity magnitude in the porous media. The similar equations stand for other two transverse directions, but transverse losses are neglected by seting the value of streamwise coefficient multiplier of 50. The source may alternatively be formulated using linear C_{R1} [kgm^{-3}s^{-1}] and quadratic C_{R2} [kgm^{-4}] resistance coefficients, as:

$$C_{\mathrm{R1}} = \frac{\mu}{K_{\mathrm{perm}}},\ C_{\mathrm{R2}} = K_{\mathrm{loss}} \frac{\rho}{2} \tag{2}$$

There are many expressions in order to evaluate pressure loss coefficient, K, and some of them are tabulated in [12]. The engineering handbook [10] provides data for our case of thickened plate (ratio of plate thickness to hydraulic diameter of the opening $t/d_h = 0.122$) and Reynolds number $\mathrm{Re} < 10^5$, in the form of resistance coefficient which represents pressure drop per unit head:

$$\zeta_{\mathrm{Re}} = \frac{2g\Delta H}{\gamma \varpi_1^2} = \left(\xi_\phi + \bar{\varepsilon}_0^{\,\mathrm{Re}} \varsigma_0 + \lambda \frac{t}{d_h} \right) \frac{1}{f^2} \tag{3}$$

where ΔH [kgm^{-2}] is the pressure loss (resistance), γ [kgm^{-3}] – the specific gravity of the flowing medium in any section, and ω_1 – the mean velocities of the stream in the conduit in front of the plate, ς_0 is determined as at $\mathrm{Re} > 10^5$:

$$\varsigma_0 = \left(0.5 + \tau\sqrt{1-f}\right)(1-f) + (1-f)^2 \tag{4}$$

For our case the Reynolds number is Re = 26452. The friction coefficient λ = 0.02965. Taking from diagram 4-11 given in [10], we obtain τ = 1.271. From eq. (4) follows ς_0 = 1.042213. From diagrams 8-2 given in [10] one find ξ_φ = 0.01598 and $\bar{\varepsilon}^{\mathrm{Re}}$ = 0.869345. From eq. (3) follows ζ_{Re} = 4.226219. The pressure drop across the perforated plate, Δp spans between the undisturbed flow upstream of the plate and a downstream location where all the effects of the plate practically vanish and at turbulent flow conditions is mainly caused by the inertial losses while assuming dissipation characteristics of the perforated plate are independent on viscous losses [8, 16, 17]. Therefore, we assumed linear resistance coefficient $C_{\mathrm{R1}} = 0$. The value of K_{loss}^S should be divided by the thickness of the plate t over which the pressure drop occur [20]. The quadratic resistance coefficient C_{R2} is:

$$C_{\mathrm{R2}} = \xi_{\mathrm{Re}} \frac{\rho}{2t} \tag{5}$$

By applying previously defined parameters for our case C1-PP from eq. (5) follows C_{R2} = 500.7 [kgm^{-4}]. Finally, the pressure drop for our case is $\Delta p = C_{\mathrm{R2}} V^2 t$ = 250.35 Pa.

It should be noted that the value of C_{R2} is related to the perforated plate with specified geometry and perpendicular inlet velocity [9, 12]. The different values of the inlet velocity as well as flow impact angles on the plate different from 90° could be the subjects of some future work.

The flow domain is divided into blocks in which unstructured meshes with different settings are created and connected by the general grid interface mesh connection method, fig. 2. A control surface approach of the numerical fluxes across the interface is used [20]. The computational mesh varied between 3.4 and 6.2 millions of cells depending on the case. An increase in the number of cell by 30% gave no noticeable influence on the values of Δp. The numerical simulations were implemented on AMD Ryzen Threadripper 3970X 32-Core Processor of 3.69 GHz clock speed and 128 GB RAM. Figure 2 shows the geometry of the flow domains of two different numerical cases denoted as C1 and C2 and position of the locations for which the results are presented in this paper, given as:

- plane P1 is y-z cross-section at x = 0.025 m (the middle of the first openings column),
- plane P2 is x-y cross-section at z = –2 m,
- plane P3 is x-y cross-section at z = 2 m,
- plane P4 is x-y cross-section at z = 6 m,

– plane P5 is *x*-*y* cross-section at z = 8 m,
– plane P6 is *x*-*z* cross-section at y = 0.04 m (the middle of the first openings row),
– line L1 is a part of *z*-axis from inlet to outlet,
– lines L2 and L3 are *x*- and *y*-axes aligned in the vertical *x*-*y* cross-section at z = 2 m respectively.

Since hydraulic diameter for the plate is D_h = 1.2 m and for the opening is d_h = 41.05 mm, the plane P2 is selected on distance of 50 d_h in the front of the plate expecting that plate does not influence upstream flow significantly yet. Plane P3 is selected on distance of 50 d_h >20 d_h behind the plate [13, 18]. Planes P2 and P3 are therefore selected in order to calculate pressure drop through the plate (dP). Plane P4 is selected on 5 D_h and plane P5 on 7 D_h behind the plate in order to investigate the level of mixing of the flow through the plate and the flow around the plate.

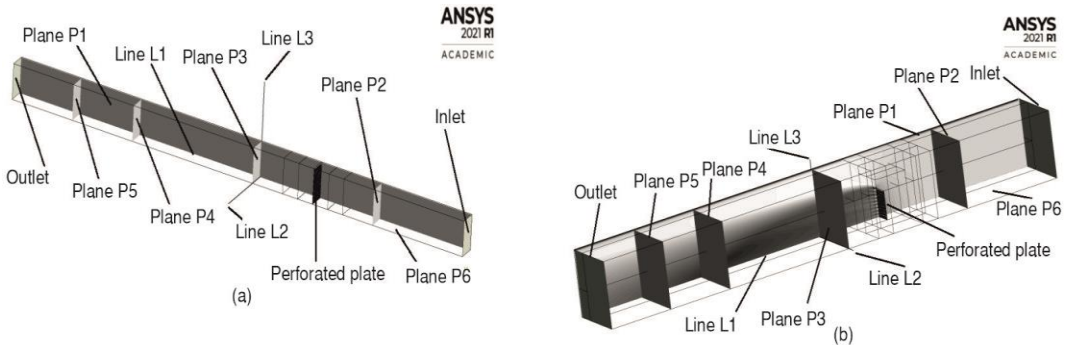

Figure 2. The geometry of the flow domains for cases C1 (a) and C3 (b)

Results and discussion

Figure 3 presents velocity component *w* distribution in planes P1, fig. 3(a), and P6, fig. 3(b), for the case C1-PP when modeling detailed geometry of the perforated plate. Through the plate openings, a sudden sharp contraction of the flow area followed by sudden enlargement appears. The vortices create behind the structure of the perforated plate and the flow structure consists of jet regions surrounded by recirculation zones, the largest of them near the channel's upper, fig. 3(a), and side, fig. 3(b), wall. Numerically obtained pressure drop for this case is $\Delta p_{\text{P2-P3}}$ = 256.7 Pa, calculated as $\Delta p_{\text{P2-P3}} = (p^{\text{ave}}_{\text{st-P2}} - p^{\text{ave}}_{\text{st-P3}})$ where $p^{\text{ave}}_{\text{st-P2}}$, $p^{\text{ave}}_{\text{st-P3}}$ are area-averaged static pressure in the planes P2 and P3, respectively. The relative deviation from the value of Δp = 250.35 Pa, calculated by using eq. (5), is 2.5%, confirming the results of the numerical simulation.

Figure 4 presents static pressure p_{st} and velocity *w* distribution on the lines L1-L3 for the case C1-PP and for cases C1-PO when perforated plate was modeled as a thin porous medium with different values of directional permeability. When changing the quadratic resistance coefficient C_{R2} from 515 to 480 kg/m^4 the pressure distribution along the lines L2 and L3 for the cases C1-PO become closer to the distribution for the case C1-PP, figs. 4(b) and 4(c). The value of p_{st} before the plate decrease resulting that pressure drop Δp decrease up to 20 Pa, fig. 4(a). A slight decrease followed by sudden pressure drop through the plate occurs in the case C1-PP, and pressure recovers after around 2 m behind the plate, fig. 4(a), while velocity *w* slightly increases in the front of the plate, suddenly decrease through the plate plane, than recovers on a value more than 10 m/s due to decrease of the flow cross-section

induced by channel's wall boundary layer effect, fig. 4(d). At the distance of around 2 m before the plate, the static pressure p_{st} and velocity w are not significantly affected by the plate.

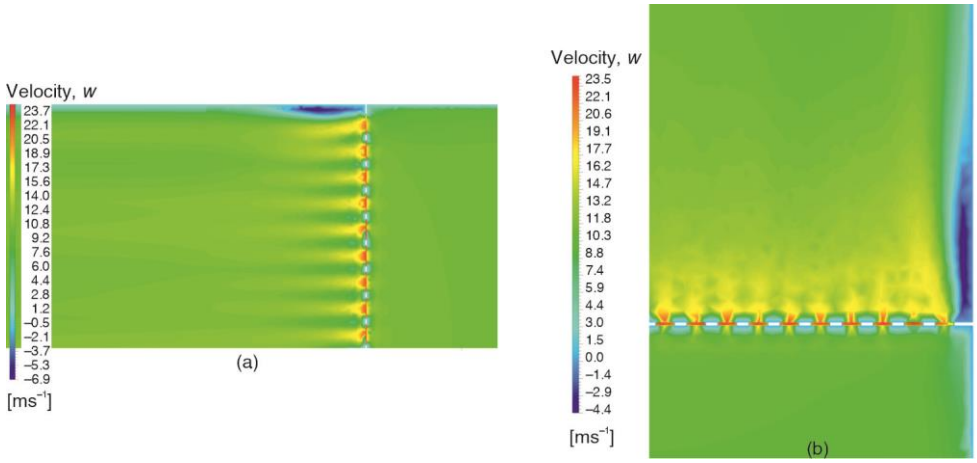

Figure 3. Contour plot of the velocity component w plane P1 (a) and P6 (b), respectively

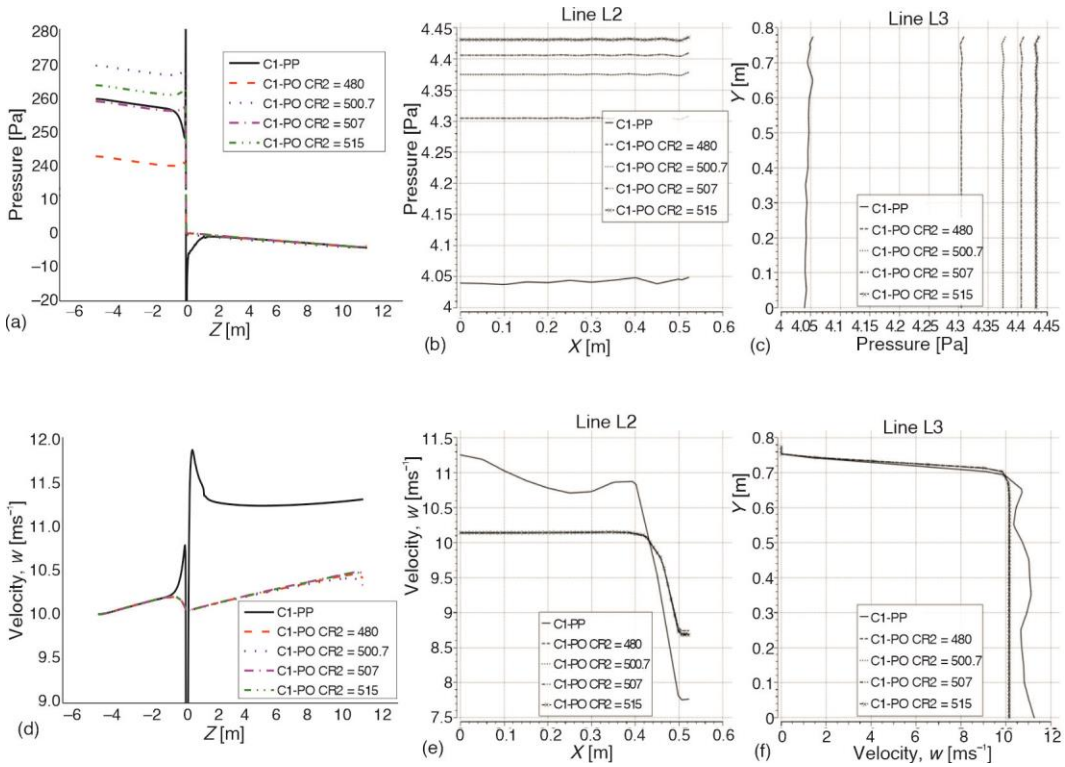

Figure 4. Static pressure p_{st} (a)-(c) and velocity w (d)-(f) distribution along the lines L1, L2, and L3, numerical cases C1-PP and C1-PO

At the distance of around 2 m after the plate, static pressure p_{st} and velocity w curves almost flattened.

Hence, for evaluating Δp we choose the position of the planes P2 and P3 on the distances 2 m in the front and after the plate, respectively. These distances are around 50 d_h for our case of a 30 × 65 mm rectangular opening and are much larger than the value of 5 d_h upstream and 20 d_h downstream as suggested by Guo *et al*. [14], or the value of 10 d_h both upstream/downstream chosen by Smierciew *et al*. [19] in their experimental set-up, both of them for the cases when palte is covering the whole cross-section of the chanell.

As expected, the porous medium model flattened the flow pattern behind the plate and velocity w pattern is not sensitive on changing C_{R2}, figs. 4(e) and 4(d). The values of pressure drop $\Delta p_{P2\text{-}P3}$ for the numerical cases C1-PO having values of C_{R2} of 480, 500.7, 507, and 515 kg/m^4 was 242.2, 252.2, 255.7, and 259.8 Pa, respectively. The case with C_{R2} = 500.7 kg/m^4 defined according to eq. (5) exhibit the best prediction of pressure drop $\Delta p_{P2\text{-}P3}$.

Figure 5 presents a contour plot of velocity w in the plane P1, fig. 5(a), static pressure p_{st} fig. 5(b) and velocity w distribution, figs. 5(c)-5(e) on the lines L1, L2, and L3 for cases C2-PP and C2-PO. The pressure drop $\Delta p_{P2\text{-}P3}$ for case C2-PP was 198.4 Pa, while in numerical cases C2-PO having C_{R2} values of 400, 500.7, and 600 kg/m^4 was 160.5, 195.7, and 229.7 Pa, respectively. According to this and to fig. 5(b), it appears that model with C_{R2} = 500.7 kg/m^4 is most acceptable. But, regarding the flow pattern behind the plate, the model with C_{R2} = 400 kg/m^4 seems to allow velocity w distribution, fig. 5(d) and 5(e), more similar to the C2-PP case. Moreover, only in that case, did the velocity w flatten up to C2-PP case at a distance of around 8 m behind the plate, fig. 5(c).

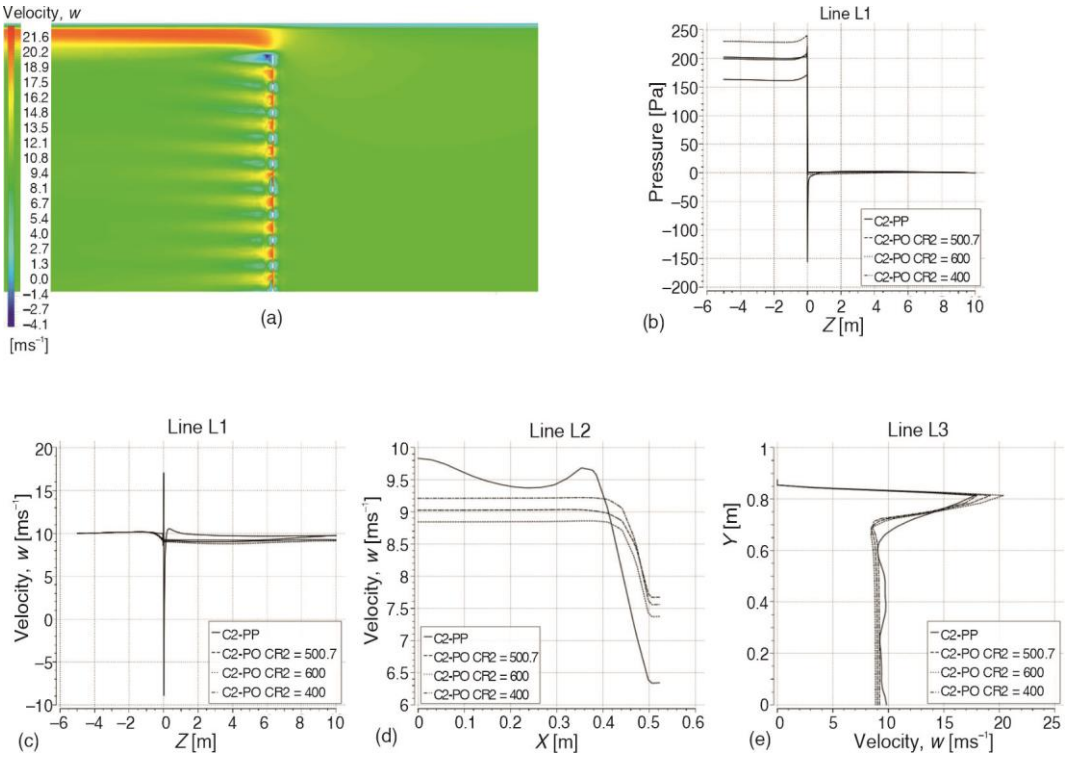

Figure 5. Velocity w contour plot, plane P1 (a), static pressure p_{st} along the line L1 (b), velocity w distribution along the lines L1, L2, and L3 (c)-(e), numerical cases C2-PP and C2-PO

Figure 6 presents a contour plot of the velocity w in the plane P1, fig. 6(a), static pressure p_{st} fig. 6(b), and velocity w distribution, figs. 6(c)-6(e), on the lines L1, L2, and L3 for the case C3-PP and cases C3-PO. Regarding the pressure distribution, the model with C_{R2} = 500.7 kg/m^4 gave the best results according to fig. 6(b) and calculated pressure drop $\Delta p_{P2\text{-}P3}$. In the case C3-PP pressure drop were 50.1 Pa, and 46.2 and 47.6 Pa in the cases C3-PO with values of C_{R2} of 500.7 and 525 kg/m^4 respectively.

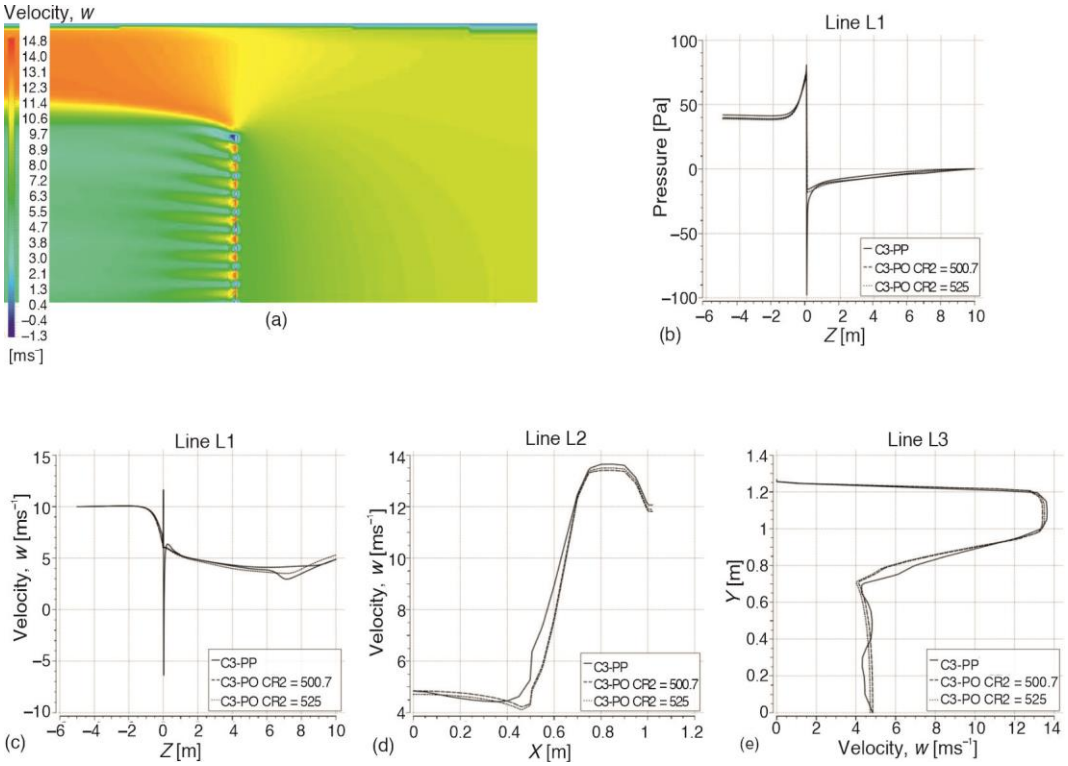

Figure 6. Velocity w contour plot plane P1 (a), static pressure p_{st} along the line L1 (b), velocity w distribution along the lines L1, L2, and L3 (c)-(e), numerical cases C3-PP and C3-PO

There is a slight improvement in the regions near the middle of the plate and near both upper and side edges of the plate regarding the velocity w distribution by using a model with C_{R2} = 525 kg/m^4 compared to the model with C_{R2} = 500.7 kg/m^4, figs. 6(c)-6(e). In the rest part of the plate, there is no significant improvement. It should be noted that further adjustment is possible, figs. 6(d) and 6(e), and that in this case further increase of C_{R2} should be checked.

Figure 7 presents a contour plot of the velocity w in the plane P1, fig. 7(a), static pressure p_{st} fig. 7(b), and velocity w distribution, figs. 7(c)-7(e), on the lines L1, L2, and L3 for the case C4-PP and cases C4-PO. A noticeable improvement in the velocity w pattern, figs. 7(d) and 7(e) as well in the pressure distribution, fig. 7(b) is obtained by using model with C_{R2} = 530 kg/m^4, slightly increased compared to the value of C_{R2} = 500.7 kg/m^4. The area of improvement is larger in the y-direction, up to 0.7 m, fig. 7(e), than in the x-direction, around 0.5 m, fig. 7(d), due to combinations of geometries of the plate and the chanell.

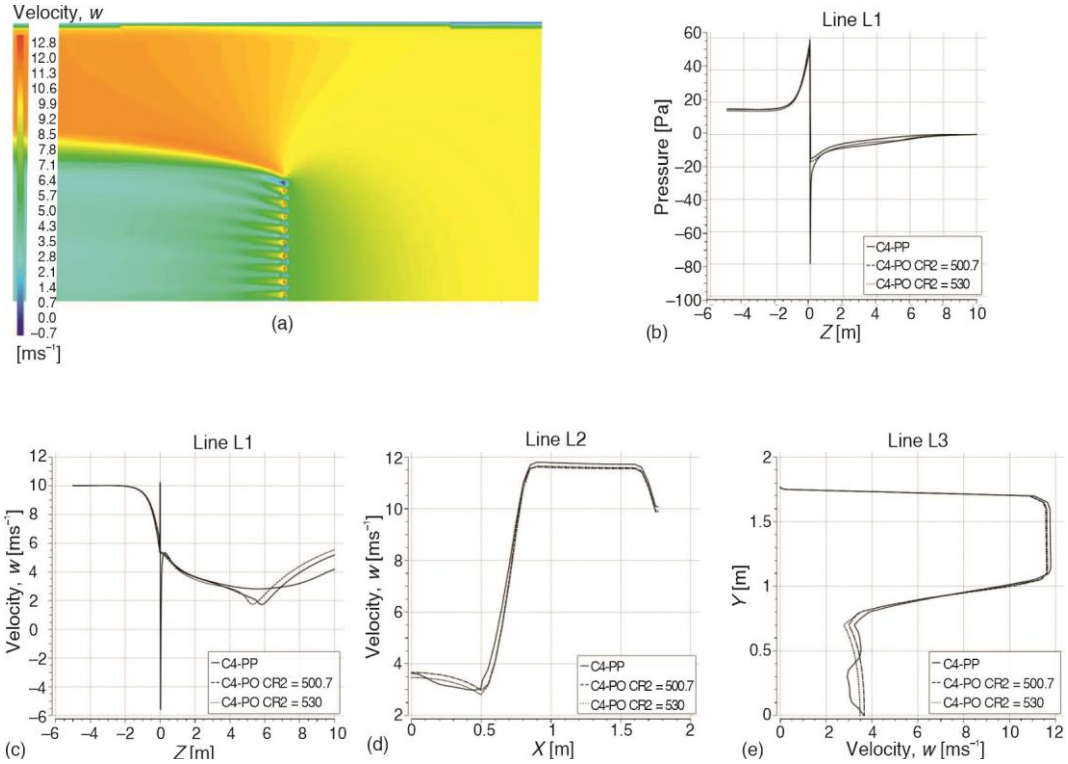

Figure 7. Velocity *w* contour plot, plane P1 (a), static pressure p_{st} along the line L1 (b), velocity *w* distribution along the lines L1, L2, and L3 (c)-(e), numerical cases C4-PP and C4-PO

Figure 8 presents a contour plot of the velocity *w* in the plane P1, fig. 8(a), static pressure p_{st} fig. 8(b), and velocity *w* distribution, figs. 8(c)-8(e), on the lines L1, L2, and L3 for the case C6-PP and cases C6-PO. A significant improvement in the velocity *w* pattern, figs. 8(d) and (e), as well in the pressure distribution, fig. 8(b), is obtained by C_{R2} = 1900 kg/m^4, higher compared to the value of C_{R2} = 500.7 kg/m^4.

Velocity *w* contour plot in the plane C1 for remaining numerical cases C5-PP and C7-PP are presented on fig. 9. Due to plate resistance to flow, the amount of the main flow changes its direction while going around the plate edges, figs. 5(a), 6(a), 7(a), 8(a), and 9.

In the region around the plate edge, the acceleration of the flow occurs, generating zones with lower static pressure that influence the flow jets emerging from the openings. The low-pressure zone induces the inclination of jets in the way that inclination is higher for jets emerging from openings closer to the plate boundaries.

The angle of jet inclination, as well amount of the flow exiting the opening, varies from the edge of the plate to the plate center. Generally, the jet inclination angle is smaller for smaller distance from the wall, fig. 5(a), Y_c = 0.1. When Y_c rises to 0.6, the low pressure zone affects the jets farther from the plate edge (closer to the plate middle) and the jet inclination angle increase to some extent. There is no noticeable increase in the jet inclination angles or further propagation of this influence on the openings closer to the middle of the plate in the case Y_c = 0.8 comparing the case Y_c = 0.6. In roughly, results indicate that the outer half of the plate area is affected. So it should be considered using the porosity varying over the plate span in the manner as proposed in [18].

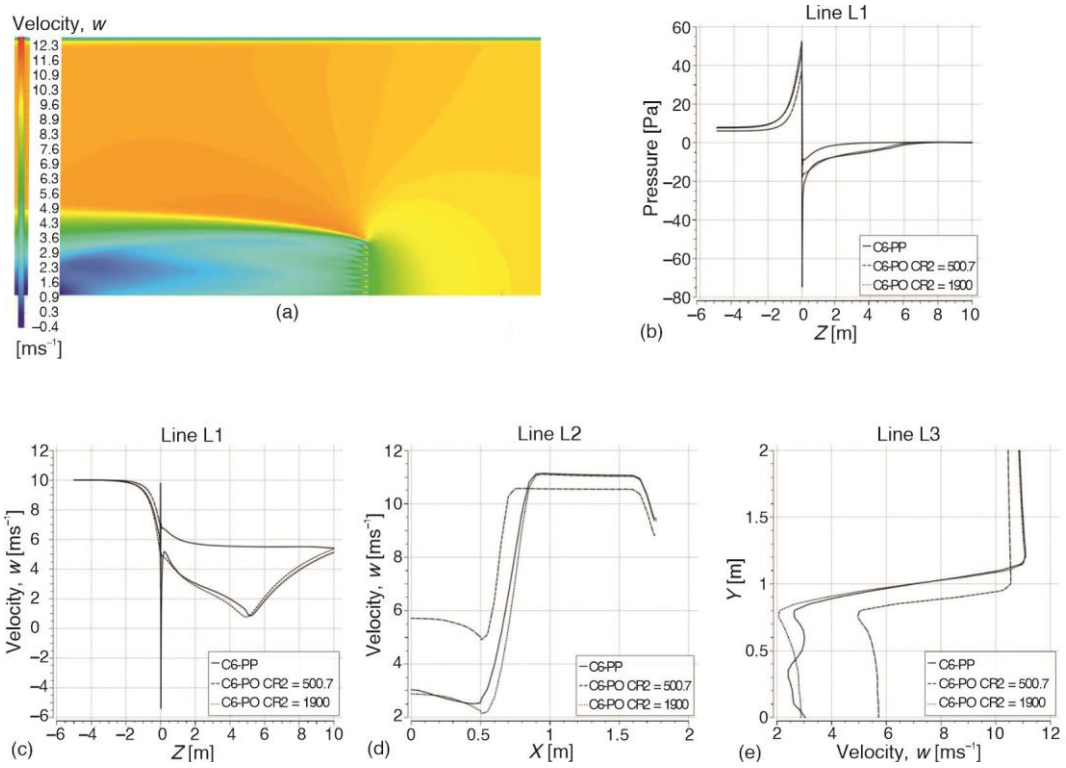

Figure 8. Velocity *w* contour plot, plane P1 (a), static pressure p_{st} along the line L1 (b), velocity *w* distribution along the lines L1, L2, and L3 (c)-(e), numerical cases C6-PP and C6-PO

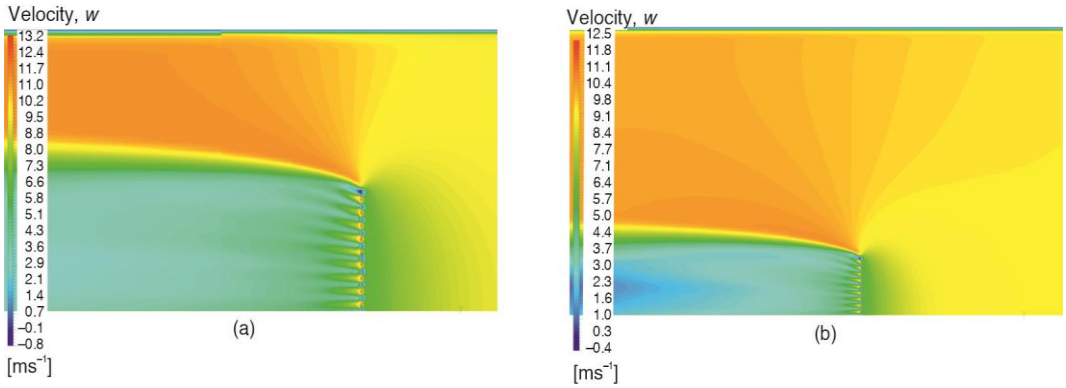

Figure 9. Velocity *w* contour plot, plane P1, numerical cases C5-PP (a) and C7-PP (b)

Conclusion

The *trial and error* iterative adjustment of the resistance coefficient when using the porous medium model in CFD simulation has been applied to resolve flow behind the perforated plate in the case when the plate is not covering the whole cross-section of the channel.

The aim was to obtain as similar as possible flow patterns behind the plate compared to the detailed modeling of the plate with openings. This study shows that a flow pattern more similar to one obtained by CFD numerical simulation of the real plate's geometry could be obtained by adjusting the resistance coefficient based on the investigation of the velocity distribution. Depending on the plate and channel geometry, the required correction in the quadratic resistance coefficient ranged from 5% to 280%. Results of this study indicate that the application of apparent instead of actual porosity could be used in resolving the problem of flow inclined to the plate. The described approach could be applied in the optimization of geometric parameters of the perforated plates or screens of one ESP when the application of the simplified porous medium model is more applicable. In order to eliminate iterative adjustment of the loss coefficient, the development of the general correlation between the resistance coefficient and statistically evaluated matching of the flow behind the plate could be the scope of future work. Besides the porosity, the influence of the gas velocity as well as plate and channel geometric parameters could be the subjects of further investigation also.

Acknowledgment

This work was financially supported by the Ministry of Education, Science and Technological Development of the Republic of Serbia, research theme: Improving the efficiency of equipment for waste gas purification and exploitation processes by increasing the fuel quality and assessing the impact on air pollution, which is being realized in VINČA Institute of Nuclear Sciences, National Institute of the Republic of Serbia, University of Belgrade, Belgrade, Serbia.

References

[1] ***, Commission Implementing Decision (EU) 2017/1442 of 31 July 2017 establishing best available techniques (BAT) conclusions, under Directive 2010/75/EU of the European Parliament and of the Council, for large combustion plants, Document 32017D1442, available online: EUR-Lex-32017D1442-EN-EUR-Lex(europa.eu), https://eur-lex.europa.eu/legal-content/EN/TXT/?uri=CELEX%3A32017D1442

[2] Veronos, A. A., *et al*., Prediction of the Cleaning Efficiency of an Electro-Static Precipitator, *Journal of Electrostatics, 55* (2002), 2, pp. 111-133

[3] Back, A., Relation Between Gas Velocity Profile and Apparent Migration Velocity in Electrostatic Precipitators, *Int. Journal of Plasma Environmental Science & Technology, 11* (2017), 1, pp. 104-111

[4] Swierczok, A., Jedrusik, M., The Collection Efficiency of ESP Model - Comparison of Experimental Results and Calculations Using Deutsch Model, *Journal of Electrostatics, 91* (2018), Feb., pp. 41-47

[5] Sahin, B., Ward-Smith, A. J., The use of Perforated Plates to Control the Flow Emerging from a Wide-Angle Diffuser, with Application to Electrostatic Precipitator Design, *International Journal of Heat and Fluid-Flow, 8* (1987), 2, pp.124-131

[6] ***, Electrostatic Precipitator Gas Flow Model Studies, Publication ICAC-EP-7, Institute of Clean Air Companies, 2004, Washington, DC, USA

[7] Sahin, B., Ward-Smith, A.J., Effect of Perforated Plates on Wide-Angle Diffuser-Exit Velocity Profiles, *Journal of Wind Engineering and Industrial Aerodynamics, 34* (1990), 2, pp. 113-125

[8] Swaminathan, M. R., Mahalakshmi, N. V., Numerical Modelling of Flow through Perforated Plates Applied to Electrostatic Precipitator, *Journal of Applied Sciences, 10* (2010), 20, pp. 2426-2432

[9] Sahin, B., et al., The Pressure Drop and Flow Charachteristics of Wide-Angle Screened Diffusers of Large Area Ratio, *Journal of Wind Engineering and Industrial Aerodynamics, 58* (1995), 1-2, pp. 33-50

[10] Idelchik, I. E., *Handbook of Hidraulic Resistance, Coefficients of Local Resistance and of Friction*, 3rd ed., Begell House, Inc, Danbury, Conn., USA, 1996

[11] Sahin, B., Pressure Losses in an Isolated Perforated Plate and Jets Emerging from the Perforated Plate, *International Journal of Mechanical Sciences, 31* (1989), 1, pp. 51-61

[12] Ozahi, E., An Analysis on the Pressure Loss Through Perforated Plates at Moderate Reynolds Numbers in Turbulent Flow Regime, *Flow Measurement and Instrumentation, 43* (2015), June, pp. 6-13

[13] Bayazit, Y., *et al*., Perforated Plates for Fluid Management: Plate Geometry Effects and Flow Regimes, *International Journal of Thermal Sciences*, *85* (2014), Nov., pp. 104-111
[14] Guo, B. Y., *et al*., Numerical Modelling of the Gas Flow Through Perforated Plates, *Chemical Engineering Research and Designe*, *91* (2013), 3, pp. 403-408
[15] Celik, N., *et al*., Design Analysis of Fluid-Flow through Perforated Plates, *Thermal Science*, *22* (2018), 6B, pp. 3091-3098
[16] Haque, S. M. E., *et al*., Flow Simulation in an Electrostatic Precipitator of a Thermal Power Plant, *Applied Thermal Engineering*, *29* (2009), 10, pp. 2037-2042
[17] Ye, X. L., *et al*., Multi-Scale Simulation of the Gas Flow Through Electrostatic Precipitators, *Applied Mathematical Modelling*, *40* (2016), 21-22, pp. 9514-9526
[18] Hosseini, S. M., *et al*., Enhancement of Gas Distribution Uniformity in a Claus Process Catalytic Reactor Using Computational Fluid Dynamics, *Chemical Engineering & Processing: Process Intensification*, *144* (2019), 107653
[19] Smierciew, K., *et al*., Numerical Prediction of Homogeneity of Gas Flow through Perforated Plates, *Processes*, *9* (2021), 10, 1770
[20] ***, Ansys CFX-Solver Theory Guide, Release 2022 R1, ANSYS, Inc.: Canonsburg, Penn., USA, 2021

Paper submitted: April 26, 2022
Paper revised: December 16, 2022
Paper accepted: December 30, 2022
© 2023 Society of Thermal Engineers of Serbia.
Published by the Vinča Institute of Nuclear Sciences, Belgrade, Serbia.
This is an open access article distributed under the CC BY-NC-ND 4.0 terms and conditions.